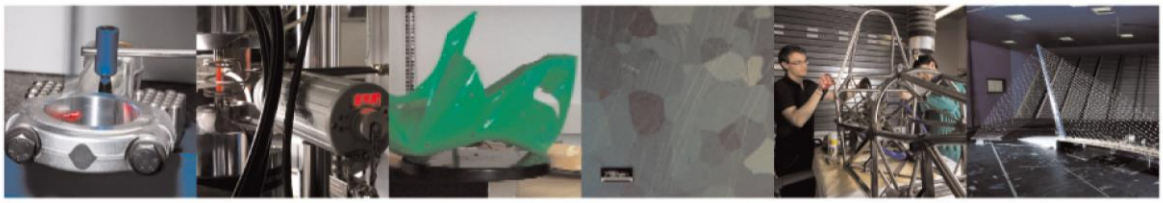

Ceramic sponge Abrasive Waterjet (AWJ) precision cutting through a temporary filling procedure

Viganò, F.; Cristiani, C.; Annoni, M.

This is a post-peer-review, pre-copyedit version of an article published in JOURNAL OF MANUFACTURING PROCESSES. The final authenticated version is available online at: http://dx.doi.org/10.1016/j.jmapro.2017.05.014

DIPARTIMENTO DI MECCANICA ■ POLITECNICO DI MILANO
via G. La Masa, 1 ■ 20156 Milano ■ EMAIL (PEC): pecmecc@cert.polimi.it
http://www.mecc.polimi.it
Rev. 0

Ceramic sponge Abrasive Waterjet (AWJ) precision cutting through a temporary filling procedure

F. Viganò[1], C. Cristiani[2], M. Annoni[1]

[1] Mechanical Engineering Department, Politecnico di Milano, Milano, Italy

[2] Chemistry, Material and Chemical Engineering Department "Giulio Natta" (CMIC), Politecnico di Milano, Milano, Italy

Corresponding author:

Francesco Viganò

Tel.: 334 3012 952

E-mail: francesco.vigano@polimi.it

ABSTRACT

Ceramic sponge machining after firing is a great issue, requiring special tools and procedures because of the material peculiar macro-structure and its intrinsic brittleness. This study approaches the problem by exploiting the Abrasive Waterjet technology (AWJ) and showing its potential as a flexible tool. Nowadays, AWJ is coming up as an alternative to other ceramic manufacturing processes such as Grinding, Ultrasonic Machining and Laser Machining. The influence of a temporary pore filling agent, infiltrated in the already sintered sponge, is evaluated and its effect on the jet coherence is investigated through both modelling and experimental approaches. The most suitable process parameters are assessed in order to reduce the main AWJ defects in these conditions, setting the feed rate (v_f) at 150 mm/min on a 35 mm thick 30 PPI (pores per inch) ceramic sponge on a conventional cutting equipment.

The overall kerf divergence is therefore reduced down to less than 1° thanks to the filling procedure and then it is compensated by exploiting a 5-axis cutting centre. Defects are measured, using both conventional and ad hoc tools (e.g. CMM, grazing light surface inspection and digital image analysis). No thermal or chemical actions are applied by the AWJ cutting process and the negligible forces exerted on the struts preserve their integrity. A case study geometry is machined, fulfilling tight tolerances of 0.1 mm on a Ø 10 mm ceramic sponge cylinder over a 15 mm thickness. A complex-shaped component is cut on 35 mm thick sponge.

KEYWORDS

Abrasive Waterjet; Ceramic sponge cutting; Temporary sponge filling; Defect compensation.

1. INTRODUCTION

High quality machining of ceramic materials is an increasingly relevant industrial issue and Abrasive Water Jet (AWJ) is becoming a well-established technology for solid ceramic cutting, as confirmed by Abdel-Rahman [1]. This study is aimed at demonstrating the AWJ process potential also in cutting near-net-shape ceramic sponge components.

A filling agent is temporarily infiltrated in the sintered sponge pores in order to preserve the ceramic sponge structure integrity from being damaged by the natural jet divergence. This novel approach can be applied to all kind of ceramic or metal sponges and is different from pre-sintering infiltration, which is useful in other cases, e.g. to enhance the sponge structure geometry during firing like in Griel [2] and Li et Al. [3], or to create composite materials by permanent infiltration as reported by Chabera et Al. [4] and Rashed et Al. [5].

The interactions between the jet and the filled sponge are tested in this paper on simple geometries and transferred to more complex case studies, where tight tolerances are required by functional purposes.

1.1. Ceramic sponges and PSM method

According to Scheffler and Colombo [6], ceramic sponges are irregular monolithic network structures characterized by open cells.

Several processes exist to fabricate ceramic sponges, including the use of pre-forming agents, partial sintering, template methods and gel-casting, as reported by Liu et al. [7]. A ceramic sponge obtained by polymeric sponge replication method (PSM) is used in the present study. In this method, patented in 1963 as reported in Brezny and Green [8], a polyvinyl chloride (PVC) sponge template is immersed in the ceramic slurry in "green" state. It is successively dried and fired like most of the ceramic artefacts, burning out the polymer structure.

Two main defects usually occur in ceramic sponges obtained by conventional PSM: the possibility to leave either a hole or a carbonaceous residue at the centre of each strut, causing cracks formation and propagation (Figure 1), and the cell deformation, causing inconsistent behaviours during the machining operations.

Figure 1 Triangular voids inside the struts caused by the PVC combustion in the 30 PPI (pores per inch) YZA selected material.

1.2. Ceramic materials machining technologies

Custom-shaped components made of solid ceramics and ceramic sponges are needed for specific applications. Since ceramic additive manufacturing is at its very early days, as in case of Song et al. [9], it is often necessary to obtain the component shape through a machining operation after sintering. The main candidate processes are listed here:

- grinding with diamond-coated tools, as reported by Malkin and Hwuan [10] and Marinescu et al. [11];
- ultrasonic machining (USM) and rotary ultrasonic machining (RUM), using abrasive slurries and ultrasonic frequency vibrating tools, as reported by Lee and Chan [12] and by Spur et al. [13];
- laser assisted machining, locally melting the target material, which is then removed by gas flows or metal tools, as reported by Marinescu [14] and Kalyanasundaram et al. [15].

All of these techniques can be successfully applied to solid ceramic workpieces, even in the case they exert a significant mechanical action.

Nevertheless, ceramic sponges are delicate networks since their compressive strength ranges from 2.60 to 23.07 MPa and their bending strength ranges from 1.20 to 11.10 MPa, according to Nor et al [16].

Grinding is the technology closest to AWJ among the ones listed before. Malkin and Hwuan [10] discussed ductile and brittle mode grinding and increased the grinding wheel speed up to 178 m/s to reduce the overall normal force per grit. This principle is enhanced by AWJ, where the actual abrasive particle speed can be three times greater (up to 550 m/s, see Section 2.3).

Therefore, the single ceramic strut is exposed to a lower stress, thus withstanding the jet action without collapsing.

2. AWJ-TARGETED CERAMIC SPONGE CHARACTERISTICS DISCUSSION

A localised material removal action without stress propagation is needed. AWJ technology already demonstrated its delicate cutting action even on thin glass and brittle materials according to Annoni et al. [17] and Hay Mohammad Jafar [18].

2.1. YZA ceramic sponge characteristics

The ceramic sponge selected for this study is a 35 mm thick SELEE Tylar XF YZA (Yttria stabilized Zirconia-Alumina), characterized by a PPI (pores per inch) index equal to 30. This size well represents the characteristic range of ceramic sponges used as catalyst supports (Twigg and Richardson [19]). Table 1 details the chemical composition and other functional characteristics of the material selected for the study.

Table 1 Main characteristics of the ceramic sponge selected for the study.

Ceramic sponge type	SELEE Tylar XF YZA
Chemical composition	Y_2O_3 / CaO / ZrO_2 / Al_2O_3 2.5% / 2.5% / 61% / 34%
Typical working temperature T [°C]	1550
Cell size [PPI]	30

2.2. Typical AWJ defects and effects on ceramic sponge

AWJ-cut components are affected by three main geometrical defects: kerf waviness, kerf taper and jet lag. In most solid ceramics, a feed rate (v_f) reduction plays a positive role on defects and increases the depth of cut as confirmed by the models of Wang [20].

Nevertheless, v_f causes conflicting effects on ceramic sponges cutting defects, as highlighted in Table 2.

Table 2 Effect of v_f reduction on the typical AWJ defects when machining different materials.

Effect of v_f reduction	Solid material	Sponge
Kerf waviness	Better	Better
Kerf taper	Better	Worst
Jet lag	Better	Better

2.3. AWJ behaviour in cutting ceramic sponge "as-is"

Inasaki [21] described the brittle behaviour of advanced ceramics in machining, especially in grinding, based on the same abrasion-erosion phenomena as in AWJ cutting. A particle hitting the workpiece surface with an impact angle close to 90° would break the ceramic sponge strut bridge without significant deformation. The abrasive particle velocity was calculated as 550 m/s according to Annoni et Al. [22], Tazibt et Al. [23] and the CFD simulations by Wang [24]. Considering this high impact speed and the low mass of a particle (6.5E-6 g/particle for #80 mesh Garnet abrasive), a single abrasive grain can only break the strut tip, without transferring the stress to the entire strut due to its low inertia. The test cut shown in Figure 2 highlights that the jet can erode the material at low v_f until replicating the jet free shape, while the resulting kerf wall is not straight at high v_f.

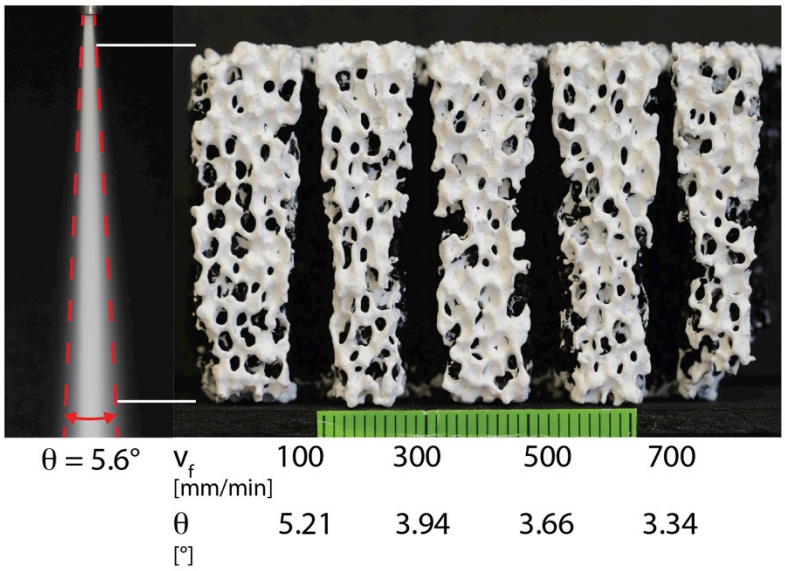

Figure 2 Actual jet shape and test specimen for the "as-is" cutting experimentation (Table 3 reports the AWJ constant process parameters applied in the current study).

Table 3 Constant AWJ process parameters applied in the current study.

Orifices Ø [mm]	Primary: 0.33 Focusing: 1.02
Water pressure [MPa]	380
Abrasive type and size	Garnet, #80 mesh
Abrasive flow rate [g/min]	350
Stand Off Distance [mm]	3
Workpiece thickness [mm]	35

This behaviour can be due to the large density difference between the solid ceramic struts and the empty pores. When passing through a pore, the jet loses its coherence and diverges assuming a less predictable behaviour.

3. CERAMIC SPONGE AND FILLED CERAMIC SPONGE CUTTING COMPARISON

Several 2D and 3D geometrical models for reticulated materials are proposed in literature. Maiti et al. [25] discussed the fracture mechanisms of brittle cellular solids, distinguishing between crack extension through bending failure and tensile failure of the cell struts in a 2D representation. A 3D modelling approach was discussed by Jang et al. [26] for polyurethane and aluminium foams, starting from the Kelvin cell representation, discussed by Thomson [27], and aiming at modelling sponge struts as shear deformable beams.

In this study, a simpler equivalent structure is used to represent filled ceramic sponges, being cut when a filling agent substitutes air inside the sponge pores (Section 3.2).

3.1. Ceramic sponge structure as a multi-layer material

The original sponge structure is converted into an equivalent multi-layer structure, preserving the ratio between solid material and empty pore along the jet axis. This simplified structure allows applying the conclusions of the studies on AWJ cutting of layered materials discussed by Hashish [28].

A X-ray Computed Tomography (CT) analysis is performed, inspecting the ceramic sponge internal geometries as made by Wallenstein et al. [29] to distinguish the solid ceramic from a fluid flow. The analysis of 1500 CT slices revealed that along the jet axis direction the solid ceramic/empty pore ratio is 3/17, the average strut thickness is 0.396 mm and the average strut number on 35 mm thick workpiece is 14 (Figure 3).

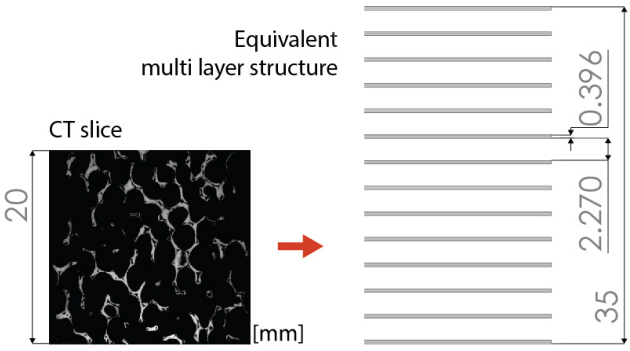

Figure 3 X-ray CT image on 20 mm thick specimen (due to micro-CT detector characteristics) and ceramic sponge equivalent multi-layer structure on 35 mm.

3.2. Jet behaviour in filled ceramic sponges

The jet is well confined when passing through the solid ceramic strut, but it can diverge when it crosses an empty pore.

A more dense filling material is exploited to replace air and preserve the jet coherence. The filling agent should effectively fill the cells, but it should be also easy-to-remove without leaving any residual. In addition, it must not be chemically reactive with the base material. For this reason, Ethylene Vinyl Acetate (EVA) is tested as filling agent. A kerf shape comparison between ceramic sponge “as-is” (Figure 4, left) and solid EVA (Figure 4, middle) is presented to evaluate the separate materials behaviour before studying the effect of their union (Figure 4, right).

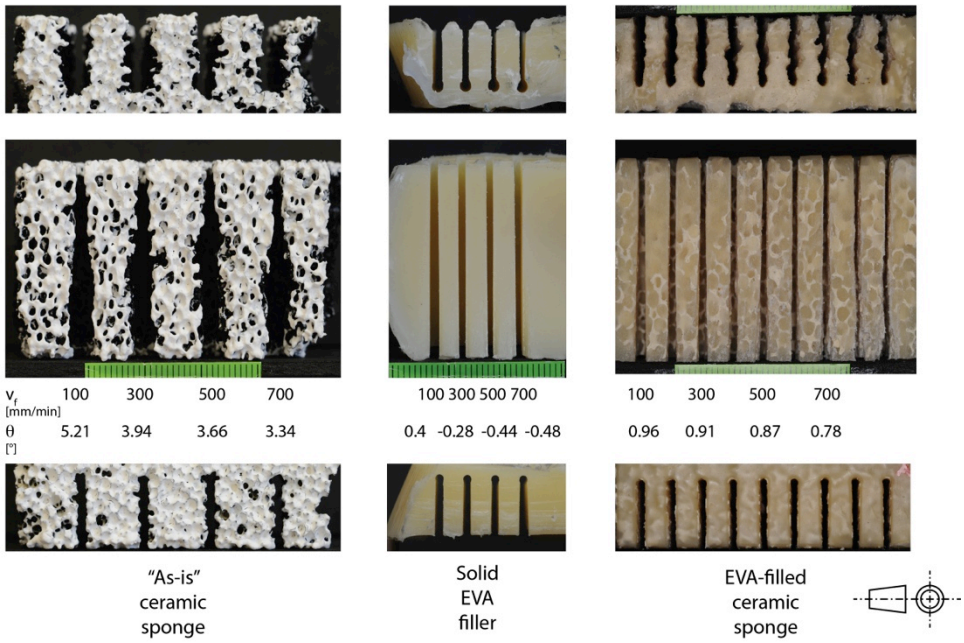

Figure 4 Comparison among "as-is", solid EVA and EVA-filled ceramic sponge cutting (constant process parameters reported in Table 3).

A superposition effect occurs in the filled specimen case. The EVA filling counteracts the jet divergence, thus reducing the overall defects and favouring the kerf shape regularity.

Figure 5 reports the divergence angle trend of the "as-is" and EVA-filled cutting conditions shown in Figure 4 in the v_f range from 100 to 700 mm/min.

This preliminary comparison, demonstrating the EVA-filling effectiveness, is followed by thorough experimental plans for waviness (Section 5.1), kerf taper (Section 5.2) and jet lag (Section 5.3) reduction.

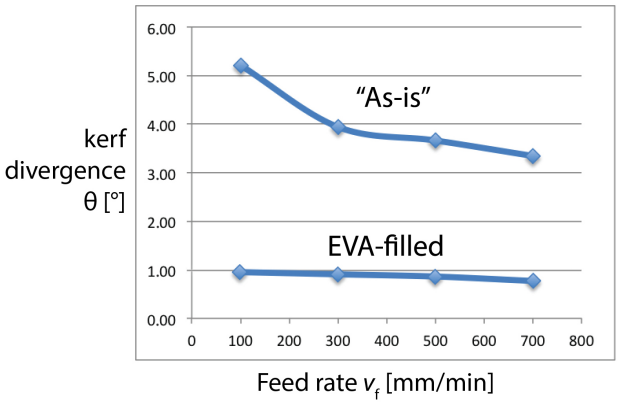

Figure 5 Kerf shape divergence comparison between "as-is" and EVA-filled ceramic sponge cutting.

4. CERAMIC SPONGE TEMPORARY FILLING PROCEDURE

4.1. Filling agent selection

Details about the filling materials are reported in Table 4.

Table 4 Main characteristics of the materials cut by the jet in the study.

Filling material	Chemical composition	Density [kg/m³]	Melting temperature T [°C]
Solid YZA ceramic	Y_2O_3 / CaO / ZrO_2 / Al_2O_3 2.5% / 2.5% / 61% / 34%	5060	2000
EVA	$(C_2H_4)_n(C_4H_6O_2)_m$	870	120

EVA is characterised by a melting temperature that is higher than the temperature generated by the jet friction, thus making it sufficiently resistant to preserve the cut wall integrity.

4.2. Temporary filling procedure assessment

The ceramic sponge workpiece is immersed in melted EVA until all the trapped air exits (Figure 6) and then it is cooled down.

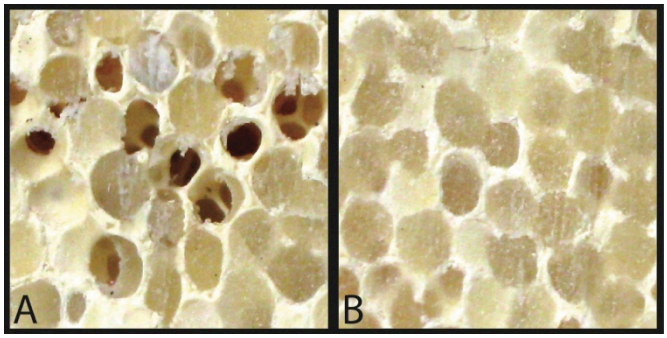

Figure 6 EVA filling procedure results. Some cells are left unfilled due to a hasty filling procedure (A), while good results are obtained carefully performing the procedure (B).

A specific removal procedure is determined to evacuate EVA from the finished part using hot oil (270 °C) to remove EVA and then cold acetone to remove the last oil traces.
A thermo-gravimetric test proves that only few EVA traces remain on the part after the described treatment (1.5% specimen weight loss at 450°C, which corresponds to the EVA degradation temperature). In any case, a calcination process is performed in the common practice immediately before using the parts, therefore removing the last non-ceramic residuals.

5. CUTTING PARAMETERS SELECTION AND DEFECT COMPENSATION

The typical AWJ defects listed in Section 2.2 are measured in this study by means of suitable procedures described in this Section.

5.1 Kerf waviness measurement and reduction

Kerf bottom waviness is strongly influenced by the ceramic sponge struts random positions. Therefore, any tool path compensations would not be effective and the only way to reduce

this defect is through an appropriate v_f selection. Kerf bottom waviness is measured by image processing (Figure 7).

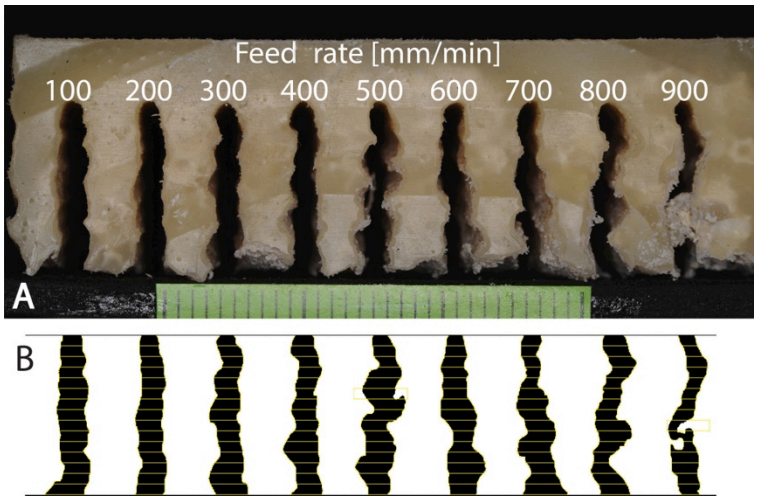

Figure 7 EVA-filled specimen bottom view (A) (v_f = 100 ÷ 900 mm/min) and processed image (B).

The single groove image is divided in 15 sub-areas, a local reference system is attributed to each sub-area and the characteristic geometric quantities are inspected (Figure 8):

- T_i is the nominal jet trajectory, where i is the groove number, from T_1 to T_9;
- X_i Y_j is the local reference system defined for each sub-area, where the origin is put on T_i at half the sub-area height (X_i ranges from X_1 to X_9 and Y_j ranges from Y_1 to Y_{15});
- C_{ij} is the sub-area centroid, calculated as the arithmetical mean of the position of each pixel belonging to the selected sub area;
- x_i and y_j are the distances between the local reference system origin (X_i Y_j) and the centroid (C_{ij}).

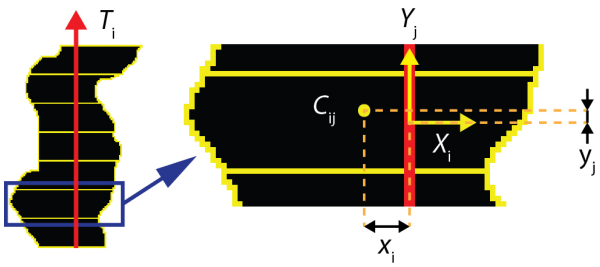

Figure 8 Representation of the geometrical analysis applied to the specimen bottom surface.

The two distance components x_i and y_j represent the groove shape regularity and therefore they are assumed as the primary cutting quality indicators.

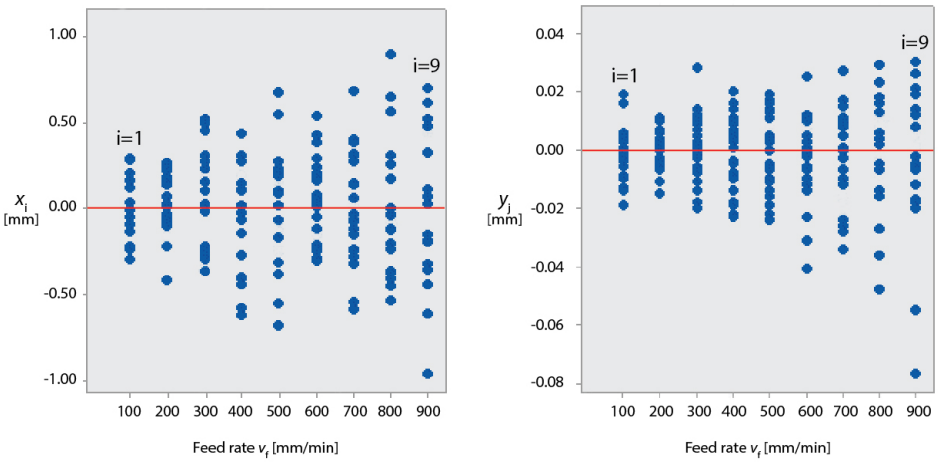

Figure 9 Scatterplot of x_i and y_i at each v_f level.

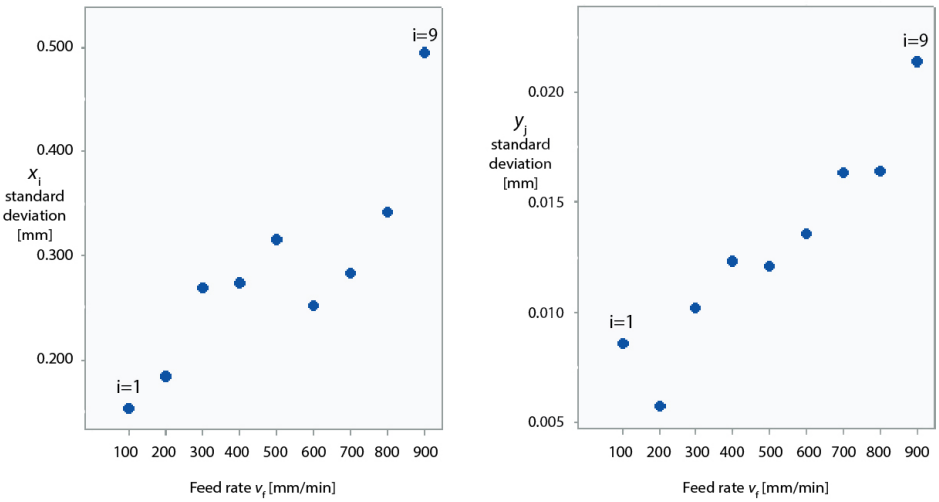

Figure 10 Scatterplot of x_i and y_i standard deviation at each v_f level.

Figures 9 and 10 show that the bottom kerf irregularity increases with v_f in all directions. Moreover, this behaviour is clearly significant in the *X* direction. The defect is two orders of magnitude greater (Figure 9, left) and less predictable (Figure 10, left) in this direction than in *Y* direction. Therefore only the lower v_f levels may be chosen and the limit v_f will be set at 150 mm/min combining this results with the ones coming from the following Section 5.2.

5.2 Kerf taper measurement and compensation

The average width of each sub-area is calculated by a dedicated routine and then all the width values belonging to the same groove are averaged. This procedure is carried out both on the top and on the bottom surfaces, thus obtaining the top and bottom widths (W_{top} and W_{bot}). Equation (1) by Annoni and Monno [30] is used to calculate the kerf taper value.

$$\text{Kerf taper} = |W_{top}\text{-}W_{bot}|/2 \quad (1)$$

The results are plotted in Figure 11.

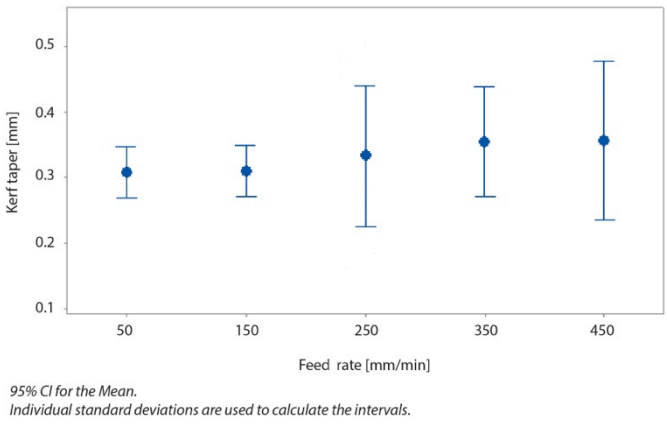

Figure 11 Interval plot for the kerf taper at each v_f level, obtained from a dedicated experimental plan in the 50-450 mm/min v_f range with the constant process parameters in Table 3.

The waviness quality weakening effect described in Section 5.1 increases the kerf taper values dispersion and makes it necessary to limit v_f to a maximum of 150 mm/min. The kerf taper is then compensated by tilting the jet.

Hoogstrate [31] applied the defect compensation strategy by managing simple geometrical parameters as the 5-axis cutting head tilt angles. The use of CAD-CAM tools enables the new machines to apply compensation strategies even in case of curved geometries, as reported by Westkämper et al. [32]. Several other studies concerning circular parts compensation are published, like the ones by Matsui [33] and Hlaváč [34].

A cut made at v_f = 150 mm/min generates a 0.3 mm taper on 35 mm thick specimens, which can be easily compensated by tilting the cutting head by 0.47° towards the scrap on a plane normal to the feed direction.

5.3 Jet lag measurement and compensation

A grazing light technique is used to reveal the jet bending effects on the surface (Figure 12).

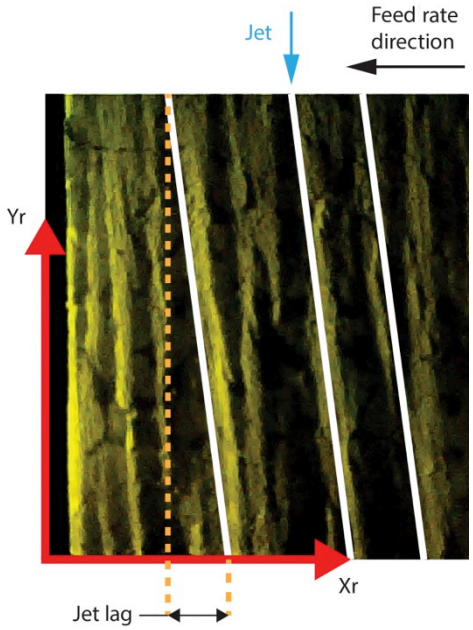

Figure 12 Jet lag measurement definition. X_r and Y_r define the reference system.

Differently from what normally observed in solid metals, the striations become straight segments in this case. The inclination is well visible and constant from the jet entrance.

The jet lag regression Equation (2) is therefore:

$$\text{jet lag [mm]} = 0.485 + 0.00348\ v_f \quad (2)$$

This equation is valid on 35 mm thick sponge for v_f values ranging from 50 to 450 mm/min and for the specific material. It returns the jet lag as the jet inlet and outlet coordinate difference along the cutting direction. At the maximum v_f allowed to avoid waviness (150 mm/min, according to Section 5.1), the jet lag is equal to 1.007 mm. This defect is compensated by tilting forward the cutting head by 1.63° along the feed direction, according to the geometric models referenced in Section 5.2 [31-34].

5.4. Defect compensation verification

Dedicated specimens were cut according to a profile made of an arc and two parallel walls (Figure 13 A) to verify the compensation effectiveness.

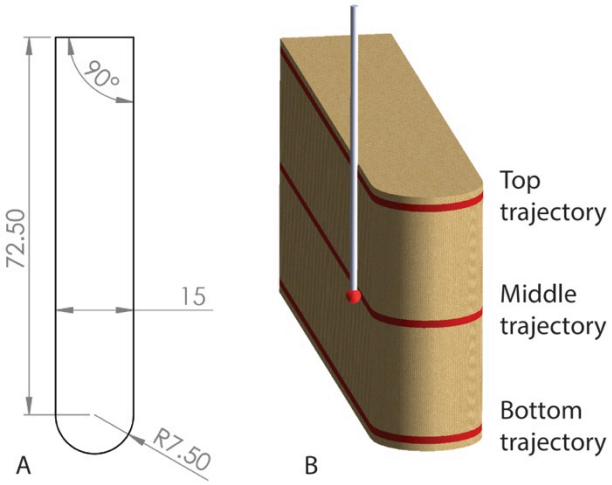

Figure 13 Compensation approach verification. Specimen sketch (A) and CMM measurement representation (B).

The specimens are measured by a Zeiss Prismo HTG CMM. The designed geometry allows verifying the compensation effectiveness (Figure 13 B).

The CMM analysis outcome points out that:

- the waviness is reduced at its minimum and it is constant along the entire thickness (straight profiles are between two parallel planes 0.05 mm far from each other);
- the taper value is reduced according to the tolerances required by the case-study (Section 6), with an error lower than 0.07 mm on the specimen thickness (parallelism) and on the arc radius at each height (top, middle and bottom) on 35 mm thick specimens;
- the jet lag is well reduced, as the 90° corners have a net shape.

6. CASE STUDY

A case study for testing the developed cutting procedure is provided by the Chemistry, Material and Chemical Engineering Department of Politecnico di Milano. The required cylinders must be stacked in a chemical reactor with internal diameter equal to Ø 10 ± 0.02 mm, therefore the component geometry is defined as shown in Figure 14. The cylinder diameter upper limit is the most important functional tolerance, therefore it is verified (Section 6.3) to prevent the cylinder from getting stuck in the pipe. The lower diameter must not be so small to avoid fluid leakage because of a large clearance between pipe and cylinder.

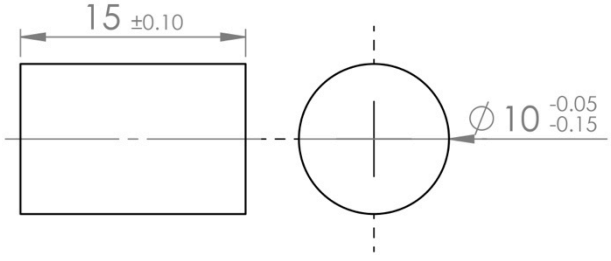

Figure 14 Case study geometry (dimensions in millimetres). Since the material is porous, the dimensions refer to the circumscribed geometrical entities.

6.1. Machining strategy

The aim of this case study is obtaining a finished part, avoiding the usual AWJ junctions between the machined component and the base material. Therefore the conventional machining path is modified as shown in Figure 15. An ad-hoc fixturing system was designed for the specific task, sustaining the machined component from the bottom.

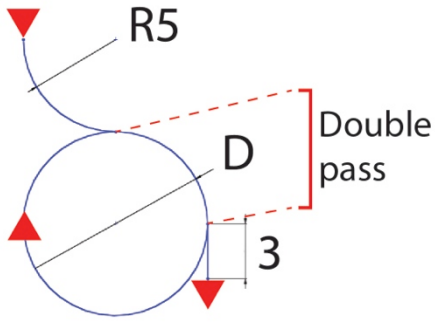

Figure 15 Modified machining path for the entrance-exit defects reduction. D is the circular trajectory diameter, adjusted according to the actual jet diameter.

The circular trajectory diameter D was automatically set by the CAD-CAM software to compensate for the jet diameter. v_f was set at 150 mm/min to reduce the waviness effects. The jet tilt angles were calculated by the taper compensation approach (Section 5.2) and by the jet lag compensation approach (Section 5.3).

6.2. Dimensional verification

The parts were functionally verified by means of a pass-gauge obtained as a 15 mm thick aluminium plate where a Ø 9.95 mm hole was carried out.

The parts cut without applying the compensation approach did not meet the defined geometrical constraints because of their conicity (Figure 16).

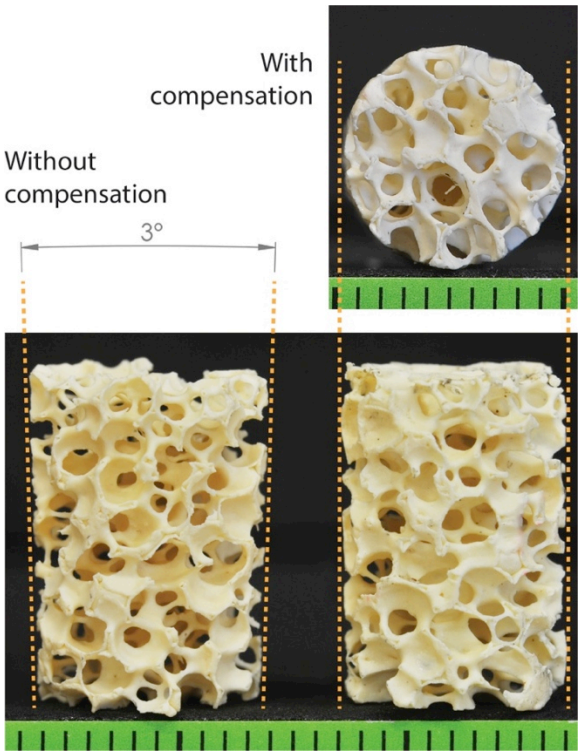

Figure 16 Case study part machined without and with the proposed compensation approach.

6.3. Complex part cutting on high thickness

A challenging part geometry was selected to test the capability of the developed cutting procedure. A star, characterized by both sharp edges and obtuse angles, was machined on the 35 mm thick filled ceramic sponge used for the current experimentation (Figure 17).

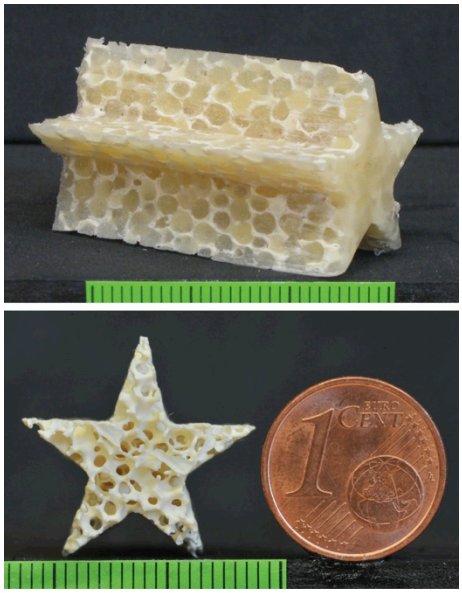

Figure 17 Demonstrative star on 35 mm thick ceramic sponge before and after filling agent removal.

The result is satisfying. In fact, it is difficult to distinguish the upper and bottom surfaces as a proof of the good performance of the compensation approach. After the filling agent removal, the fragile sharp edges of the star tips are effectively preserved (Figure 17, front view).

7 CONCLUSIONS

This study demonstrates the capability of AWJ technology to machine ceramic sponges producing high precision parts. This result is obtained thanks to the development of a temporary filling procedure. The effectiveness of the AWJ cutting performances on filled ceramic sponges is shown by case studies characterized by tight tolerances and hard-to-machine geometrical features.

The proposed process parameters (v_f = 150 mm/min, P = 380 MPa) allow obtaining precise parts, thus complying with tight dimensional and geometric tolerances and fulfilling the functional needs. A conventional 5-axis AWJ cutting system is suitable for near-net-shape

ceramic sponge parts cutting, using the proper filling procedure to preserve the fragile structure integrity.

From the part production point of view, the experimentation is now being extended to finer PPI ceramic sponges, more complex geometries and advanced handling systems for 3D cutting and shaping.

The application field of the AWJ technology on ceramic sponge processing will therefore be widened, getting the access to energetic and biomedical applications.

8 ACKNOWLEDGEMENTS

The authors wish to thank the WJ_Lab staff, especially Manuele Preda and Giacomo Didoni, for the innovative ideas provided for this study and Riccardo Balzarotti, for his expertise in the field of catalytic processes and equipment.

The authors are grateful to Stefano Petrò and AMALA Laboratory (Milano) for the CT analysis, and to Alessandra Pighi, Valerio Mussi and Massimo Goletti, MUSP Consortium (Piacenza), for the image analysis.

9 REFERENCES

[1] Abdel-Rahman A A. An Abrasive water jet Model for Cutting Ceramics. In Proceedings of the International Conference on Mathematical Models for Engineering Science, 2010 (pp. 978-960).

[2] Greil P. Near net shape manufacturing of polymer derived ceramics. Journal of the European Ceramic Society, 1998, 18(13), 1905-1914.

[3] Li J, Zhang X H, Cui B C, Lin Y H, Deng X L, Li M, & Nan C W. Mechanical performance of polymer-infiltrated zirconia ceramics. Journal of Dentistry 2017, 58, 60-66.

[4] Chabera P, Boczkowska A, Witek A, & Oziębło A. Fabrication and characterization of composite materials based on porous ceramic preform infiltrated by elastomer. Bulletin of the Polish Academy of Sciences Technical Sciences, 2015, 63(1), 193-199.

[5] Rashed A, Yazdani M, Babaluo A A, & Hajizadeh Parvin P. Investigation on high-velocity impact performance of multi-layered alumina ceramic armors with polymeric interlayers. Journal of Composite Materials, 2016, 50(25), 3561-3576.

[6] Scheffler M, Colombo P. Cellular ceramics: structure, manufacturing, properties and applications. John Wiley & Sons 2006.

[7] Liu R, Li Y, Wang C A & Tie S. Fabrication of porous alumina–zirconia ceramics by gel-casting and infiltration methods. Materials & Design 2014, 63, 1-5

[8] Brezny R and Green DJ. Factors Controlling the Fracture Resistance of Brittle Cellular Materials. Journal of the American Ceramic Society 1991, 74(5):1061 - 1065

[9] Song X, Chen Y, Lee TW, Wu S, Cheng L. Ceramic fabrication using Mask-Image-Projection-based Stereolithography integrated with tape-casting. Journal of Manufacturing Processes 2015, 20, 456-464.

[10] Malkin S and Hwang TW. Grinding mechanisms for ceramics. CIRP Annals-Manufacturing Technology 1996, 45(2), 569-580.

[11] Marinescu ID, Spanu CE, Hitchiner M. Double sided grinding of advanced ceramics with diamond wheels. IDR. Industrial diamond review 2006, (4).

[12] Lee TC, Chan CW. Mechanism of the ultrasonic machining of ceramic composites. Journal of materials processing technology 1997, 71(2), 195-201.

[13] Spur G, Uhlmann E, Holl S. Ultrasonic machining of ceramics. Handbook of Advanced Ceramics Machining 2006, 327-353.

[14] Marinescu ID. Laser-assisted grinding of ceramics. Interceram 1998, 47(5), 314-317.

[15] Kalyanasundaram D, Shrotriya P, Molian P. Fracture mechanics-based analysis for hybrid laser/waterjet (LWJ) machining of yttria-partially stabilized zirconia (Y-PSZ). International Journal of Machine Tools and Manufacture 2010, 50(1), 97-105.

[16] Nor MAAM, Hong LC, Ahmad ZA, Akil HM. Preparation and characterization of ceramic foam produced via polymeric foam replication method. Journal of materials processing technology 2008, 207(1), 235-239.

[17] Annoni M, Arleo F, Viganò F, Villa L, Volpi S. Abrasive Waterjet micro machining of Non-conventional Materials for Industrial Applications. Proceedings of the 4M/ICOMM 2015 conference 2015, 455-458

[18] Jafar RHM, Nouraei H, Emamifar M, Papini M, Spelt JK. Erosion modeling in abrasive slurry jet micro-machining of brittle materials. Journal of manufacturing processes 2015, 17, 127-140.

[19] Twigg MV, Richardson JT. Preparation and properties of ceramic foam catalyst supports. Studies in Surface Science and Catalysis 1995, 91, 345-359.

[20] Wang J. A new model for predicting the depth of cut in abrasive waterjet contouring of alumina ceramics. Journal of Materials Processing Technology 2008, 209(5), 2314-2320.

[21] Inasaki I. Grinding of hard and brittle materials. CIRP Annals-Manufacturing Technology 1987, 36(2), 463-471.

[22] Annoni M, Cristaldi L, Norgia M, Svelto C. Efficiency Measurement of Water Jet Orifices by a Novel Electrooptical Technique. IEEE Transactions on Instrumentation and Measurement 2008, 47(1), 48-54

[23] Tazibt A, Parsy F, Abriak N. Theoretical analysis of the particle acceleration process in abrasive water jet cutting. Computational Materials Science 1995, 5, 243-254

[24] Wang J. Particle velocity models for ultra-high pressure abrasive waterjets. Journal of Materials Processing Technology 2009, 209(9), 4573-4577.

[25] Maiti SK, Ashby MF, Gibson LJ. Fracture toughness of brittle cellular solids. Scripta Metallurgica 1984, 18(3), 213-217.

[26] Jang WY, Kraynik AM, Kyriakides S. On the microstructure of open-cell foams and its effect on elastic properties. International Journal of Solids and Structures 2008, 45(7), 1845-1875.

[27] Thomson W. Philosophical Magazine 1887, 24, 503

[28] Hashish M. A modeling study of metal cutting with abrasive waterjets. Journal of Engineering Materials and Technology 1984, 106(1), 88-100.

[29] Wallenstein M, Hafen N, Heinzmann H, Schug S, Arlt W, Kind M, Dietrich B. Qualitative and quantitative insights into multiphase flow in ceramic sponges using X-ray computed tomography. Chemical Engineering Science 2015, 138, 118-127.

[30] Annoni M, Monno M. A lower limit for the feed rate in awj precision machining. BHR group conference series publication 2000, 41, 285-296

[31] Hoogstrate AM. Towards High-Definition Abrasive Waterjet Cutting-A model based approach to plan small-batch cutting operations of advanced materials by high-pressure abrasive waterjets. TU Delft, Delft University of Technology 2000.

[32] Westkämper E, Henning A, Radons G, Friedrich R, Ditzinger T. Cutting Edge Quality Through Process Modeling of the Abrasive Waterjet. CIRP, Proceedings of 2nd CIRP International, June 2000, 21-23.

[33] Matsui S. High precision cutting method for metallic materials by abrasive waterjet. Jetting Technology 1991.

[34] Hlaváč LM. Investigation of the abrasive water jet trajectory curvature inside the kerf. Journal of Materials Processing Technology 2009, 209, 4154–4161.

LIST OF FIGURES

LIST OF TABLES